Can magnetic fabrics distinguish between aseismic and seismic slip along faults?

R. Issachar[1], T. Levi[1] and R. Weinberger[1,2]

[1]Geological Survey of Israel, Jerusalem, Israel

[2]Department of Geological and Environmental Sciences, Ben Gurion University of the Negev, Beer Sheva, Israel

Key Points

(1) Magnetic fabrics are analyzed near faults in order to distinguish between aseismic and seismic slips.

(2) Analysis demonstrates two end-member types of magnetic fabrics - symmetric and unchangeable vs. asymmetric and changeable.

(3) Magnetic fabrics near aseismic and seismic faults are different and enable to distinguish between slip histories.

Abstract

A long-standing problem in paleoseismic studies is to distinguish between aseismic and seismic slips along faults. We address this problem by characterizing the magnetic fabrics of rock samples around mesoscale normal faults of aseismic origin, and comparing them to those around co-seismic normal faults. Detailed sampling profiles along traverses, <0.2 m up to ~20 m from both sides of the faults, indicate symmetric and unchangeable magnetic fabrics of deformation origin that are coaxial with the regional strain field. These results are essentially different from magnetic fabrics detected around co-seismic normal faults, which show fault-related fabrics with asymmetric and changeable orientations. The analysis demonstrates two end-member cases of

magnetic fabrics in association with aseismic and seismic slips along faults. We suggest that magnetic fabric analysis provides a powerful and efficient tool to characterize inelastic deformation around faults, enabling to distinguish between seismic and aseismic slip histories.

Plain Language Summary

A long-standing problem in the study of Earth's deformation is to differentiate between faults that originate during earthquake evens (seismic faults) and those that are creeping due to long-lasting, regional stresses (aseismic faults). We address this problem by characterizing the magnetic fabrics of rock samples around faults of aseismic origin and compare them with magnetic fabrics around faults of seismic origin. The magnetic fabrics mimics the distribution of minerals and grains in the rocks, and, hence, are commonly served as a tool to detect "order" and "disorder" in rocks. The results indicate that around the aseismic faults the magnetic fabrics are uniform and reflect the large-scale regional deformation, whereas around the seismic faults the magnetic fabrics are changeable and reflect the local deformation along the faults. Since all the faults were formed under similar sedimentary conditions, we demonstrate two end-member cases of magnetic fabrics in association with aseismic and seismic slips along faults. We suggest that magnetic fabric analysis provides a powerful and efficient tool to characterize inelastic deformation around faults, enabling us to distinguish between seismic and aseismic slip histories.

1. Introduction

Faults are common geological features reflecting deep and shallow crustal processes and, as such, are used to decipher different geological environments. Faults accumulate displacement by slow aseismic slip (creep) at plate tectonic rates (10^{-12} to 10^{-10} m/s) or by fast seismic slip of earthquake rates (10^{-4} to 10 m/s). There are several suggested criteria to recognize seismic slip along faults, including pseudotachylytes that form during frictional heating, pulverized rocks that form by transient stresses at the rupture tip (Rowe and Griffith, 2015), and fault-related texture of hematite (Ault, 2020). Nevertheless, seismic slip does not necessarily leave distinct petrological traces in the host rock, especially in cases where the rupture reaches close to the surface. The characteristics of host-rock deformation around faults have the potential to categorize their associated slip histories (Faulkner et al., 2010). Inelastic deformation within the host rock is expected to form already before and during the early stages of fault formation and growth (Anderson, 1951; Scholz, 2002). Field observations (e.g., Kim et al., 2004; Crider and Peacock, 2004; Di Toro et al., 2005; Faulkner et al., 2010), models of quasi-static (e.g., Pollard and Segall, 1987) and dynamic rupturing (Ben-Zion and Shi, 2005; Johri et al., 2014) show that zones of inelastic deformation develop around propagating faults for both aseismic and seismic slips, but in different ways (e.g., Faulkner et al., 2010). In the aseismic case, inelastic deformation would develop on both sides of the fault (i.e., symmetrical deformation), and might be related to the regional strain field (Figure 1a.1; e.g. Peng and Johnson, 1972). Alternatively, the aseismic slip would lack a prominent fault-related deformation zone (Figure 1a.2). In the seismic case, inelastic deformation would form mainly on one side of the fault (i.e., asymmetrical deformation), with relation to changeable stress field due to fault directivity and strain perturbations (Figure 1b; Ben-Zion and Shi, 2005; Ma and Andrews, 2010; Johri et al.,

2014). The potential of distinguishing between seismic and aseismic slips by characterizing the geometry and distribution of the deformation around faults was previously explored mainly by the distribution of brittle deformation markers such as veins, joint sets or microcracks (Faulkner et al., 2010), yet it is not always clear which marker best portrays the zone of inelastic deformation.

In this study, we characterize the zone of inelastic deformation around faults using anisotropy of magnetic susceptibility (AMS)-based magnetic fabric analysis, aiming to distinguish between aseismic and seismic origins of the faults. The AMS analysis has commonly been used for quantifying inelastic deformation in sedimentary rocks (Parés, 2015). The magnetic fabrics reflect the preferred alignment of crystals and grain shapes within a rock sample and, as such, provide a powerful tool to characterize intrinsic deformation on a grain scale (Borradaile and Jackson, 2010; Weinberger et al., 2017). Various intra- and inter-crystalline deformation mechanisms contribute to the AMS, such as grain boundary sliding, dislocation glide, twinning, and kinking (Evans et al., 2003). These mechanisms produce irreversible deformation without destruction of the lattice integrity, and thus, magnetic fabrics provide a sensitive tool to assess inelastic deformation even prior to the development of macroscopic brittle deformation (e.g., Larrasoaña et al., 2011). Another chief advantage of the AMS analysis for petrofabric characterization is the averaging out of large numbers of grains over the whole volume of the sample (~10 cm^3).

Previous works showed that magnetic fabrics in fault zones may developed during slow geological processes as well as short and fast events such as earthquakes (Levi et al., 2006, 2014; Casas-Sainz et al., 2018; Marcén et al., 2019; Elhanati et al., 2020). To test the applicability of AMS to diagnose aseismic and seismic slips, we compare the magnetic fabrics around faults of

two end-member origins: (1) faults of known aseismic slip that represent slow and shallow crustal deformation (Figure 1a), and, (2) faults of proven seismic slip origin that represent earthquake-driven fast crustal deformation (Figure 1b). Levi et al. (2014) and Elhanati et at. (2020) show that magnetic fabrics near co-seismic normal faults within the seismically-active Dead Sea Fault (DSF) system indicate fault-related magnetic fabrics, explained in terms of dynamic rupturing. In this study, we characterize the magnetic fabrics near normal faults that represent shallow crustal deformation of aseismic origin. The comparison of the magnetic fabrics around these two end-member types of faults allows us to test the hypothesis that the zone of inelastic deformation around aseismic and seismic faults is essentially different and can be distinguished by AMS analysis.

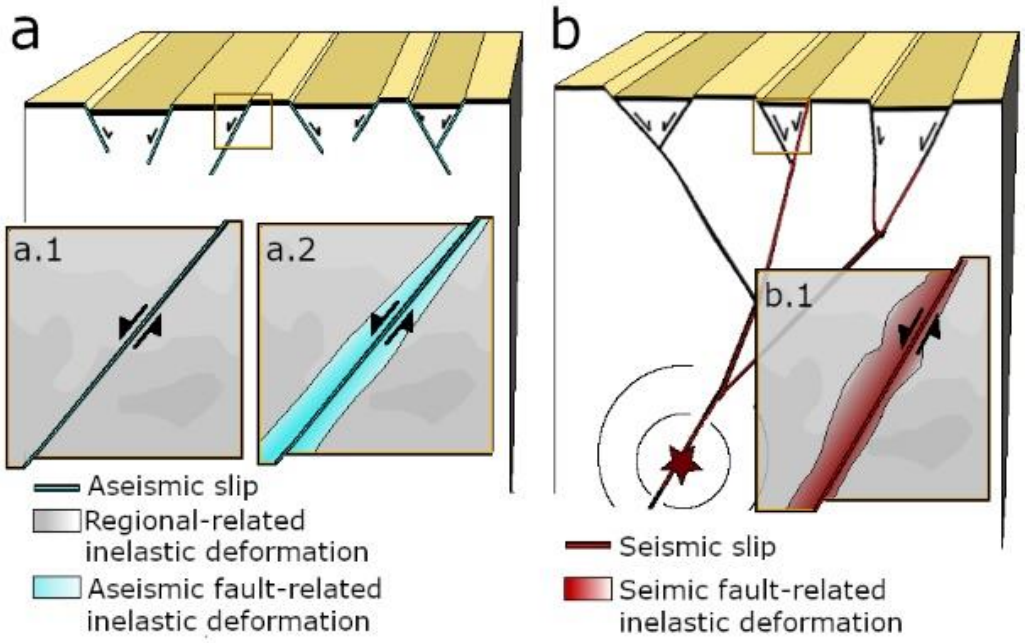

Figure 1. Structural setting of two end member types of faults and their associated inelastic deformation: (a) Faults of aseismic origin represent shallow crustal deformation with regional strain-related inelastic deformation (a.1), or fault-related inelastic deformation distributed symmetrically on both sides of the fault (a.2). (b) Faults of seismic origin connected to a deep-seated hypocenter. The red

lines represent rupture propagation during a single event. Fault-related deformation is distributed asymmetrically along one side of the fault.

2. Magnetic Fabrics

Magnetic fabrics describe the rock magnetic susceptibility tensor (**k**) with maximum, intermediate, and minimum principal susceptibility axes - $\mathbf{K_1}$, $\mathbf{K_2}$, and $\mathbf{K_3}$, respectively, which correspond to $k_1 \geq k_2 \geq k_3$ eigenvalues (Rochette et al., 1992; and reference therein). Studies of the magnetic fabrics of weakly deformed sedimentary rocks indicate that the orientation of the principal susceptibility axes (AMS axes) are related and coaxial to the principal strain (or stress) axes. Under sedimentary and compaction processes, $\mathbf{K_3}$ axes align perpendicular to bedding and $\mathbf{K_2}$ and $\mathbf{K_1}$ axes are scattered on a plane parallel to bedding (Type I, deposition and compaction; Parés, 2015). In weakly tectonically deformed rocks, $\mathbf{K_1}$ axes are often oriented along the intersection of bedding and the tectonic flattening plane, whereas $\mathbf{K_3}$ axes align perpendicular to bedding (Type II, deformation). During slow progressive deformation, the magnetic fabrics often show clusters of all three principal axes, and the $\mathbf{K_1}$, $\mathbf{K_2}$, and $\mathbf{K_3}$ axes are coaxial with the minimum ($\boldsymbol{\varepsilon_3}$), intermediate ($\boldsymbol{\varepsilon_2}$) and maximum ($\boldsymbol{\varepsilon_1}$) shortening axes, respectively (Type III, deformation; Borradaile and Jackson, 2010).

We use AMS data measured at room temperature (RT-AMS) as the main method for characterizing the magnetic fabrics of the chalk sample. RT-AMS was measured at a low magnetic field of 450 A/m and a frequency of 976 Hz with a KLY-4S Kappabridge (AGICO Inc.) at the Geological Survey of Israel. To correlate the RT-AMS with specific minerals, we use several experimental techniques, including measurements of AMS at low temperatures of ~77 K (LT-AMS), anisotropy of anhysteretic remanence magnetization (AARM), vibrating sample magnetometer (VSM) hysteresis loops, alternating field demagnetization curves (AF curves) and

temperature-dependent ($k_{(T)}$) susceptibility measurements. Experiments were performed at the Geological Survey of Israel and at the Institute for Rock Magnetism, University of Minnesota. The parameters used to characterize the magnetic fabrics, including the mean susceptibility ($k_m=[k_1+k_2+k_3]/3$), degree of anisotropy ($P=k_1/k_3$), shape of anisotropy ($T=ln(F)-ln(L)/ln(F)+ln(L)$), magnetic lineation ($L=k_1/k_2$) and magnetic foliation ($F=k_2/k_3$) were calculated according to Jelinek (1981) using the Anisoft 4.2 software package (www.agico.com).

3. Geologic Setting and Sampling

We study two normal faults of aseismic origin within the Beer Sheva syncline. The syncline is an approximately 100 km-long, ~35 km-wide that was formed during the Eocene under long-lasting compressional regional stress field of NW maximum horizontal compression, denoted σH_{NW} (Figure 2b) (Bahat, 1988; Levi et al., 2019). The Beer Sheva syncline is located within the Sinai subplate and is spatially remote (60 km) from the active DSF system and any other known active faults (Figure 2a) (Kurzon and Wetzler, 2019). Faults and joint sets were formed during burial in the poorly consolidated pelagic chalk sediments at shallow depths (Buchbinder et al., 1988) and represent paleostress regimes that are associated with the formation and uplift episodes of the syncline (Bahat et al., 2005).

The studied faults (hereafter Fault A and Fault B) are exposed along the banks of Secher Creek at the Beer Sheva syncline and are located ~120 m apart (Figure 2c). The faults cut chalks of the middle Eocene Maresha Formation (Figure 2d) (Buchbinder et al., 1988). The ~10 m exposed surfaces of the faults are accompanied by a few mm of fine-grained gouge layers. The faults trend differently with an angle of 90° between their strikes: Fault A dips NW (52°/310°; dip/dip direction) and is striking subparallel to the syncline axis; Fault B dips NE (41°/040°) and is striking perpendicular to the syncline axis (Figure 2c and figure 3). The throw of both faults is

147 approximately 3.5 m. The faults are considered to form under wet conditions in the early burial
148 stages of the chalks during the formation of the Beer Sheva syncline (Buchbinder et al., 1988).

149 The studied chalks of the Maresha Formation have high porosity (>20%) (Palchik & Hatzor,
150 2002) and may contain up to 25% clay fraction (Nathan and Flexer, 1977). A previous AMS and
151 rock magnetic study of this formation demonstrates that the rocks contain pure diamagnetic
152 carbonate coccolith as the rocks matrix, paramagnetic clays (palygorskite and smectite), and
153 minor quantities of low-coercivity ferromagnetic Fe oxides (Issachar et al., 2018).

154 To construct the magnetic fabric profiles, we collected standard (25x25 mm) cylindrical core
155 samples along horizontal cross-sections, <0.2 m up to ~20 m from both sides of the tested faults
156 (Figure 2c). In addition, we sampled a reference outcrop, located ~50 m away from the faults
157 (Figure 2c). By this strategy, we provide a high-resolution “continuous" view of the inelastic
158 strain field around the faults. The sampling strategy allows us to diagnose three different
159 scenarios of magnetic fabrics: (1) regional-related fabrics, that are uniformly distributed on both
160 sides of the tested faults; (2) fault-related fabrics that are symmetrically distributed on both sides
161 of the fault with similar orientations of AMS axes within each block (i.e., unchangeable
162 distribution); and (3) fault-related fabrics that are developed asymmetrically mainly on one side
163 of the fault with varying orientations of AMS axes (i.e., changeable distribution).

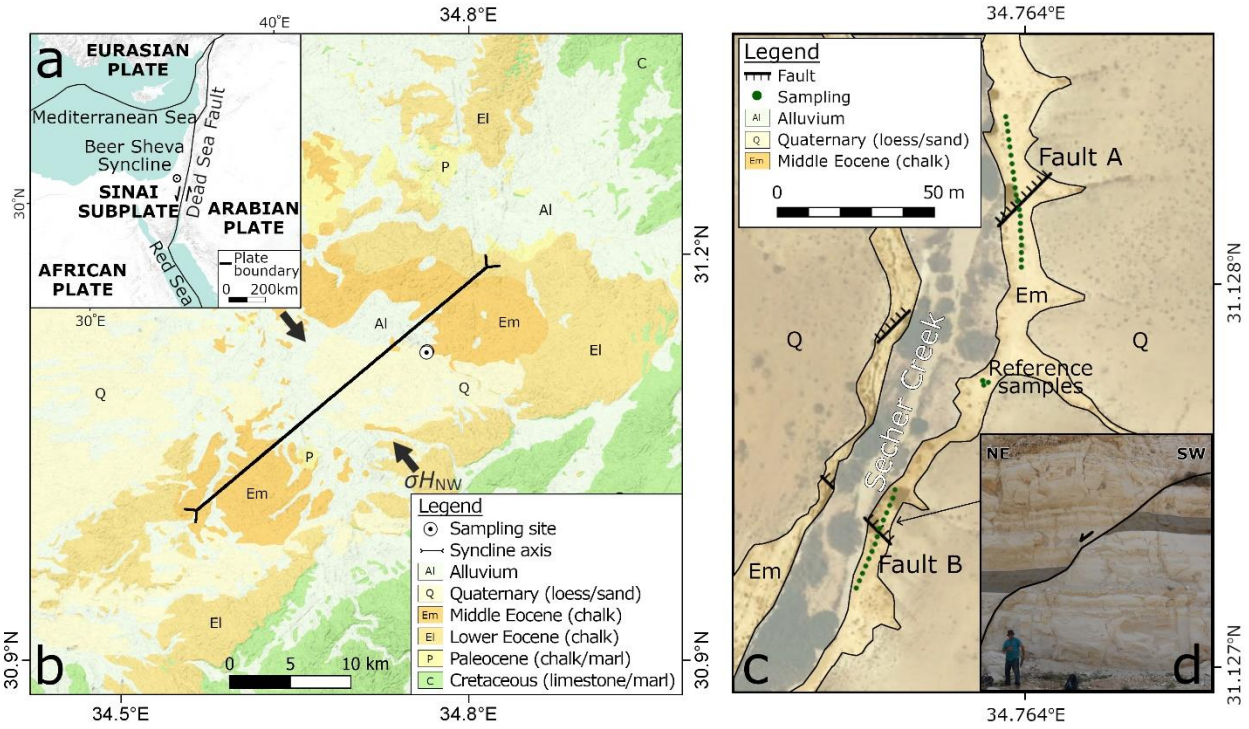

Figure 2. (a) General tectonic map of the study area. The circle marks the location of Beer Sheva syncline. (b) Geological map of the Beer Sheva syncline, showing Cretaceous to Quaternary strata (after Sneh et al., 1998), the syncline axis (after Bahat et al., 2005) and the direction of the regional stress field of σH_{NW}. (c) Detailed geological map of the study area, showing the fault traces cutting the middle Eocene strata and the distribution of the samples next to the faults (for more details see supporting information Table S1). (d) Photograph of Fault B showing an apparent fault dip and throw.

4. Results and Discussion

RT-AMS measurements of 111 chalk samples near the two tested faults indicate a narrow range of susceptibility values between 4 and 36 ($\times 10^{-6}$ SI) with a mean of 17 ± 7 ($\times 10^{-6}$ SI). The narrow range of the susceptibility values indicates that the samples has uniform mineralogy. The LT-AMS mean susceptibility value is 88 ± 21 ($\times 10^{-6}$ SI), indicating amplification factors of 4.6 ± 0.4 (supporting information Figure S1), and suggests that both paramagnetic and diamagnetic minerals contribute to the rocks susceptibility (Issachar et al., 2018). VSM hysteresis loops indicate positive linear response between -1 and 1 T. Yet, slope-corrected curves suggest minor

presence of low-coercivity ferromagnetic minerals. AF demagnetization curves indicate that most of the remanent magnetization (up to 90%) is lost by a demagnetization field up to 60 mT, suggesting that mostly low-coercivity minerals carry the remanent magnetization. Temperature-dependent susceptibility curves indicate minor susceptibility changes during heating, suggesting minor contribution of ferromagnetic minerals to the rocks susceptibility. Hence, we conclude that the rocks predominantly contain diamagnetic carbonate minerals and paramagnetic clay minerals with negligible presence of ferromagnetic minerals (supporting information Figure S2), in accordance with previous magnetic fabrics of chalks from the area (Issachar et al., 2018).

LT-AMS and AARM fabrics show insignificant anisotropy and inconsistent orientations of susceptibility axes, suggesting that neither paramagnetic nor ferromagnetic minerals are the carriers of the RT-AMS (supporting information Figure S3 and Figure S4). The insignificant anisotropies of the LT-AMS and AARM, the negligible ferromagnetic contribution and the dominance of diamagnetic minerals (i.e., calcite) suggest that the RT-AMS is controlled by the orientation distribution of the diamagnetic calcite minerals. Previous studies have shown that the orientation of the AMS axes of calcite are sensitive strain indicators with $\mathbf{K_3}$ axes parallel to the compaction/shortening direction (e.g., Owens and Rutter, 1978; de Wall et al., 2000; Almqvist et al., 2010; Issachar et al., 2018).

The orientation of the AMS axes of the studied chalk samples indicate deformation fabrics of Type II, which is characterized by tight clusters of $\mathbf{K_3}$ axes oriented sub-perpendicular to bedding, and moderate to tight clusters of $\mathbf{K_1}$ and $\mathbf{K_2}$ axes within the bedding plane (Figure 3). The AMS axes of samples collected from distance of <0.2 m up to 20 m from both sides of the tested faults, as well as from the reference outcrop have similar and consistent orientations with NE-SW trending $\mathbf{K_1}$ axes and NW-SE trending $\mathbf{K_2}$ axes (Figure 3). The $\mathbf{K_1}$ and $\mathbf{K_2}$ axes are

202 syncline parallel and syncline perpendicular, respectively, and are compatible with the syncline-
203 driven σH_{NW} stress field. Notably, irrespective to the attitude of the faults, the AMS axes around
204 them are similar and parallel to the syncline axes. In that sense, the AMS axes indicate uniform,
205 unchangeable distribution of inelastic deformation that is associated with the regional stress
206 field. The anisotropy *P* and shape *T* have values of 1.005 ± 0.003 and of 0.2 ± 0.4, respectively
207 (supporting information Figure S5 and Table S1). The AMS parameters show perceptible
208 differences between the blocks of the faults (supporting information Figure S5). The parameters
209 *P* and *L* have higher values in the footwall of Fault A and in the hanging wall of Fault B. The
210 shape of anisotropy is oblate (*T~1*) in the hanging wall of Fault A and is neutral (*T~0*) in its
211 footwall and in both blocks of Fault B. The *F* parameter shows no significant differences
212 between the blocks. The variations in the AMS parameters may imply that strain magnitudes
213 locally develop differently between the faulted blocks.

214 Fault observations and experiments show that inelastic deformation develops in association with
215 the regional stress field prior to host-rock faulting (e.g., Scholz, 1968; Mollema and Antonellini,
216 1999; Wilson et al., 2003; Crider and Peacock, 2004; Paterson and Wong, 2005; Blenkinsop,
217 2008). The faults of the current study are considered to form under wet conditions in the early
218 burial stages of the chalks (Buchbinder et al., 1988). The low strength of the chalks at the time of
219 the syncline formation could explain the absence of prominent fault-related deformation during
220 aseismic (i.e., creeping) slips on the faults. Hence, we suggest that the AMS axes represent the
221 regional stress (strain) field during the formation of the syncline and were already acquired prior
222 to the formation of the faults.

223 Contrary to the present findings, AMS studies of co-seismic faults within the active DSF system
224 infer prominent fault-related magnetic fabrics (Levi et al., 2014; Elhanati, 2019). Figure 4

presents the AMS results near two tested normal faults of a proven seismic origin (Marco et al., 1996). The faults cut late Pleistocene soft sediments in the Masada Plain, Israel and are associated with throw of ~2 m that occurred during single earthquake events (Marco and Agnon, 2005). The two tested faults were propagated throughout low-strength sediments, close to the surface and under wet conditions (Marco et al., 1996). Several AMS characteristics are well explained in terms of dynamic rupturing: (1) fault-related fabrics are asymmetrically distributed between the fault blocks; (2) the orientation of AMS axes is changeable and occasionally compatible with the principal strain directions defined by the fault focal-plane solutions; and (3) the width of the deformation AMS fabric zone is roughly similar to the amount of displacement during a single slip event. The faults in the Beer Sheva syncline and in the DSF system are comparable as they have similar throw and were developed in low strength carbonate sediments at shallow depth under wet conditions. The comparison of the magnetic fabrics of these two end-member type of faults shows clearly that only the seismic faults form a prominent fault-related magnetic fabrics (Figure 5a and Figure 5c). Nevertheless, we do not dispute the possible formation of fault-related magnetic fabrics around aseismic faults that would differ from those around seismic faults (Figure 5b).

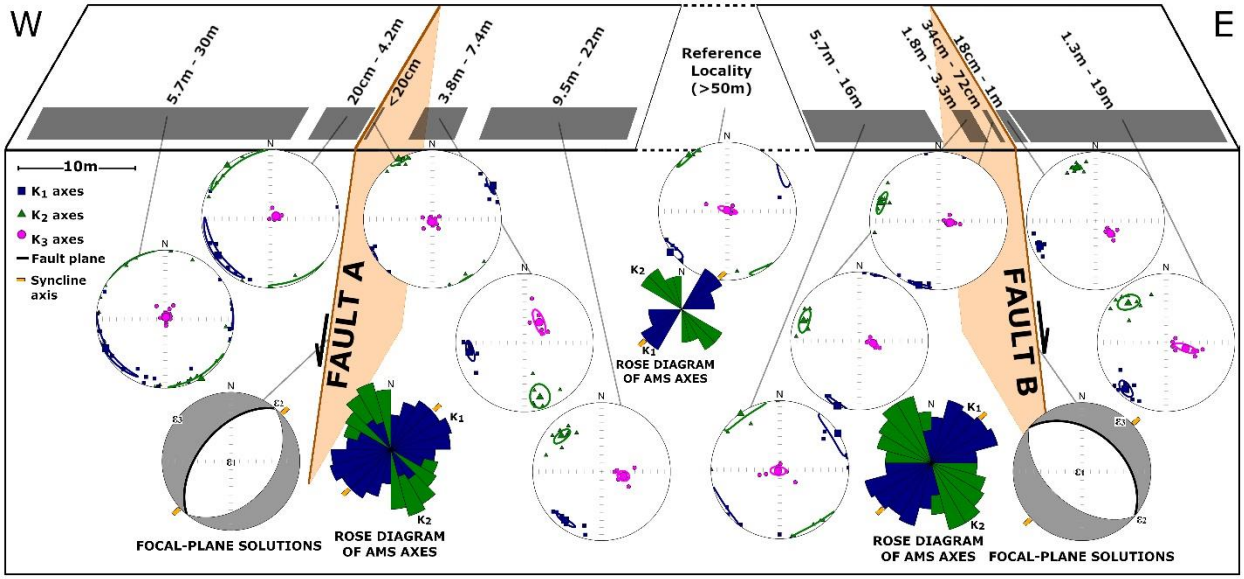

241

242 **Figure 3.** RT-AMS magnetic fabrics from sites at varied distances from aseismic faults (Fault A and Fault
243 B) in the Beer Sheva syncline. Stereoplots are lower-hemisphere, equal-area projection of AMS principal
244 axes, and the 95% confidence ellipses. The AMS axes show clustering of three principal axes indicating
245 deformation origin. Rose diagrams show that the $\mathbf{K_1}$ axes trend NE-SW parallel to the syncline axis
246 (yellow line), and the $\mathbf{K_2}$ axes trend NW-SE perpendicular to the syncline axis. Focal-plane solutions for
247 the studied normal faults are indicated with ε, ε_2, and ε_3 are the infinitesimal maximum, intermediate
248 and minimum principal strain axes, respectively.

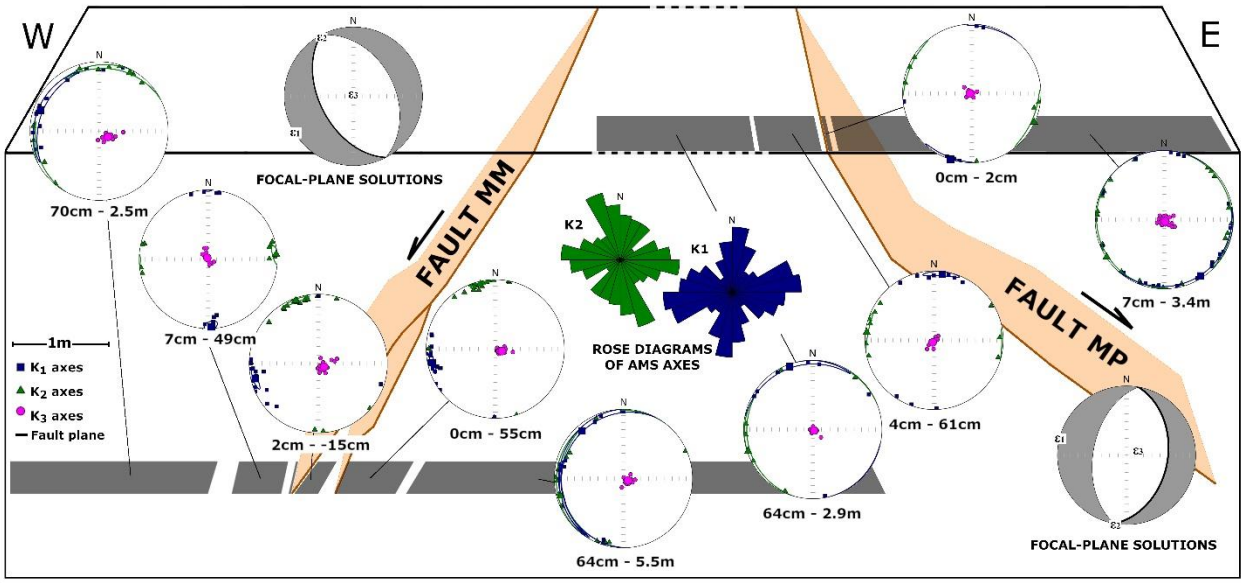

Figure 4. RT-AMS magnetic fabrics from sites at varied distances from co-seismic faults (Fault MM and Fault MP) in the Dead Sea Fault system, after Levi et al. (2014). The AMS axes show changeable orientations and asymmetrically distribution between the fault blocks. See Figure 3 for definition of steroplots and focal-plane solutions.

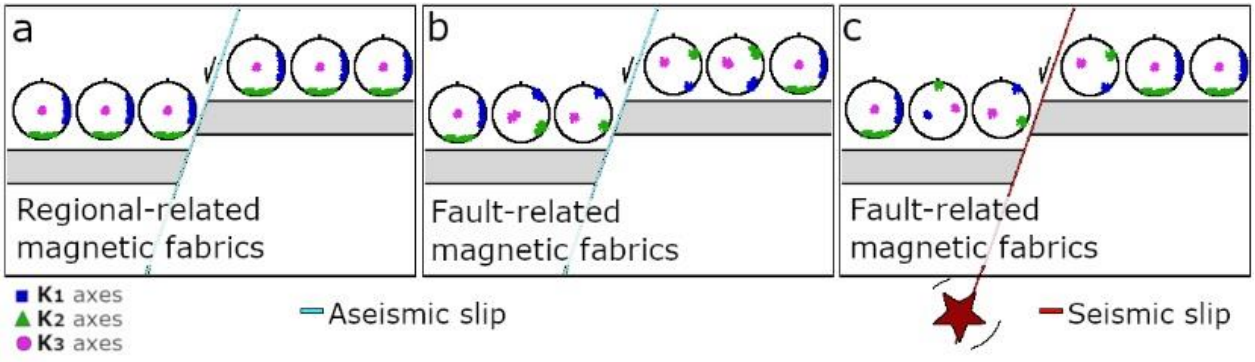

Figure 5. Conceptual model for AMS axes around faults. (a) Fault of aseismic origin showing AMS axes that are related only to the regional strain field. (b) Fault of aseismic origin with fault-related AMS axes on both sides of the fault, indicating an unchangeable strain field in each block. (c) Faults of seismic origin showing fault-related AMS axes mainly on one side of the fault, which indicate a changeable strain field. Note that away (>50 m) from the faults in (b) and (c), the magnetic fabrics could be of type I (deposition, compaction).

5. Conclusions

We measured the magnetic fabrics around two mesoscale faults of aseismic origin. The results show robust and consistent magnetic fabrics of deformation origin, implying that AMS provides a sensitive deformation marker to study inelastic deformation in the host rock. The orientation of the AMS axes indicate symmetric and unchangeable magnetic fabrics of deformation origin on both sides of the studied faults, showing a strong association with the syncline axis and the regional strain field. The symmetrical and unchangeable regional-related magnetic fabrics are compatible with observations and models of strain field around aseismic fault formation. The present results were compared with previous magnetic fabric around co-seismic faults that also formed in low strength sediments at shallow depths under wet conditions. Next to these fault, the magnetic fabrics are changeable and asymmetrically distributed. In light of the current results and previous aforementioned magnetic fabric studies, we suggest that magnetic fabric analysis provides a powerful and sensitive tool to characterize inelastic deformation around faults. We highlight the new possibility of using magnetic fabric analysis to distinguish between aseismic and seismic slip histories.

6. Acknowledgments

This study was supported by the Israel Science Foundation (ISF grant No. 868/17) and by a grant from the Israeli Government under Geological Survey of Israel DS project 40706.

The data used in this paper are available for download at:
https://figshare.com/s/c6331844fa5cdf0580c5.

7. References

Almqvist, B.S.G., Herwegh, M., Schmidt, V., Pettke, T., and Hirt, A.M., 2010, Magnetic susceptibility as a tool to study deformed calcite with variable impurity content: Geochemistry Geophysics Geosystems, v. 11, doi:Q01z0910.1029/2009gc002900.

Anderson, E.M., 1951, The dynamics of faulting and dyke formation with applications to Britain: Oliver and Boyd.

Ault, A.K., 2020, Hematite fault rock thermochronometry and textures inform fault zone processes: Journal of Structural Geology, v. 133, p. 104002, doi:10.1016/j.jsg.2020.104002.

Bahat, D., 1988, Early single-layer and late multi-layer joints in the Lower Eocene chalks near Beer Sheva, Israel: Annales Tectonicae II, p. 3–11.

Bahat, D., Rabinovitch, A., and Frid, V., 2005, Tensile Fracturing in Rocks: Heidelberg, Springer, 251–279 p., doi:2004108439.

Ben-Zion, Y., and Shi, Z., 2005, Dynamic rupture on a material interface with spontaneous generation of plastic strain in the bulk: Earth and Planetary Science Letters, v. 236, p. 486–496, doi:10.1016/J.EPSL.2005.03.025.

Blenkinsop, T.G., 2008, Relationships between faults, extension fractures and veins, and stress: Journal of Structural Geology, v. 30, p. 622–632, doi:10.1016/J.JSG.2008.01.008.

Borradaile, G.J., and Jackson, M., 2010, Structural geology, petrofabrics and magnetic fabrics (AMS, AARM, AIRM): Journal of Structural Geology, v. 32, p. 1519–1551, doi:10.1016/j.jsg.2009.09.006.

Buchbinder, B., Benjamini, C., Mimran, Y., and Gvirtzman, G., 1988, Mass transport in Eocene pelagic chalk on the northwestern edge of the Arabian platform, Shefela area, Israel:

Sedimentology, v. 35, p. 257–274, doi:10.1111/j.1365-3091.1988.tb00948.x.

Casas-Sainz, A.M. et al., 2018, Strain indicators and magnetic fabric in intraplate fault zones: Case study of Daroca thrust, Iberian Chain, Spain: Tectonophysics, v. 730, p. 29–47, doi:10.1016/J.TECTO.2018.02.013.

Crider, J.G., and Peacock, D.C., 2004, Initiation of brittle faults in the upper crust: a review of field observations: Journal of Structural Geology, v. 26, p. 691–707, doi:10.1016/J.JSG.2003.07.007.

Elhanati, D., 2019, Characterizing the strain field around co-seismic faults using magnetic fabrics (MSc Thesis): Tel Aviv University.

Elhanati, D., Levi, T., Marco, S., and Weinberger, R., 2020, Zones of inelastic deformation around surface ruptures detected by magnetic fabrics: Tectonophysics, v. 788, p. 228502, doi:10.1016/j.tecto.2020.228502.

Evans, M.A., Lewchuk, M.T., and Elmore, R.D., 2003, Strain partitioning of deformation mechanisms in limestones: examining the relationship of strain and anisotropy of magnetic susceptibility (AMS): Journal of Structural Geology, v. 25, p. 1525–1549, doi:10.1016/S0191-8141(02)00186-4.

Faulkner, D.R., Jackson, C.A.L., Lunn, R.J., Schlische, R.W., Shipton, Z.K., Wibberley, C.A.J., and Withjack, M.O., 2010, A review of recent developments concerning the structure, mechanics and fluid flow properties of fault zones: Journal of Structural Geology, v. 32, p. 1557–1575, doi:10.1016/J.JSG.2010.06.009.

Issachar, R., Levi, T., Marco, S., and Weinberger, R., 2018, Separation of Diamagnetic and Paramagnetic Fabrics Reveals Strain Directions in Carbonate Rocks: Journal of

Geophysical Research: Solid Earth, v. 123, p. 2035–2048, doi:10.1002/2017JB014823.

Jelinek, V., 1981, Characterization of the magnetic fabric of rocks: Tectonophysics, v. 79, p. T63–T67, doi:10.1016/0040-1951(81)90110-4.

Johri, M., Dunham, E.M., Zoback, M.D., and Fang, Z., 2014, Predicting fault damage zones by modeling dynamic rupture propagation and comparison with field observations: Journal of Geophysical Research: Solid Earth, v. 119, p. 1251–1272, doi:10.1002/2013JB010335.

Kim, Y.-S., Peacock, D.C.., and Sanderson, D.J., 2004, Fault damage zones: Journal of Structural Geology, v. 26, p. 503–517, doi:10.1016/J.JSG.2003.08.002.

Kurzon, I., and Wetzler, N., 2019, Defining and mapping capable tectonic sources for seismic hazard estimation in Israel: general analysis and specific focus for nuclear power plants in Israel. Report GSI/21/15. Geological Survey of Israel (2015).:

Larrasoaña, J.C., Gómez-Paccard, M., Giralt, S., and Roberts, A.P., 2011, Rapid locking of tectonic magnetic fabrics in weakly deformed mudrocks: Tectonophysics, v. 507, p. 16–25, doi:10.1016/j.tecto.2011.05.003.

Levi, T., Avni, Y., and Bahat, D., 2019, Evolution of the stress field near the Arava basin located along the Dead Sea Fault system as revealed by joint sets: Journal of Structural Geology, v. 128, p. 103876, doi:10.1016/J.JSG.2019.103876.

Levi, T., Weinberger, R., Aïfa, T., Eyal, Y., and Marco, S., 2006, Injection mechanism of clay-rich sediments into dikes during earthquakes: Geochemistry, Geophysics, and Geosystems, v. 7, p. Q12009 (doi:10.1029/2006GC001410).

Levi, T., Weinberger, R., and Marco, S., 2014, Magnetic fabrics induced by dynamic faulting reveal damage zone sizes in soft rocks, Dead Sea basin: Geophysical Journal International,

v. 199, p. 1214–1229, doi:10.1093/gji/ggu300.

Ma, S., and Andrews, D.J., 2010, Inelastic off-fault response and three-dimensional dynamics of earthquake rupture on a strike-slip fault: Journal of Geophysical Research, v. 115, p. B04304, doi:10.1029/2009JB006382.

Marcén, M., Román-Berdiel, T., Casas-Sainz, A.M., Soto, R., Oliva-Urcia, B., and Castro, J., 2019, Strain variations in a seismogenic normal fault (Baza Sub-basin, Betic Chain): Insights from magnetic fabrics (AMS): Tectonophysics, v. 765, p. 64–82, doi:10.1016/J.TECTO.2019.05.014.

Marco, S., and Agnon, A., 2005, High-resolution stratigraphy reveals repeated earthquake faulting in the Masada Fault Zone, Dead Sea Transform: Tectonophysics, v. 408, p. 101–112.

Marco, S., Stein, M., Agnon, A., and Ron, H., 1996, Long term earthquake clustering: a 50,000 year paleoseismic record in the Dead Sea Graben: J. Geophys. Res., v. 101, p. 6179–6192.

Mollema, P.N., and Antonellini, M., 1999, Development of strike-slip faults in the dolomites of the Sella Group, Northern Italy: Journal of Structural Geology, v. 21, p. 273–292, doi:10.1016/S0191-8141(98)00121-7.

Nathan, Y., and Flexer, A., 1977, Clinoptilolite, paragenesis and stratigraphy: Sedimentology, http://onlinelibrary.wiley.com/doi/10.1111/j.1365-3091.1977.tb01919.x/abstract (accessed September 2015).

Owens, W.H., and Rutter, E.H., 1978, The development of magnetic susceptibility anisotropy through crystallographic preferred orientation in a calcite rock: Physics of the Earth and Planetary Interiors, v. 16, p. 215–222,

http://www.sciencedirect.com/science/article/pii/0031920178900146.

Parés, J.M., 2015, Sixty years of anisotropy of magnetic susceptibility in deformed sedimentary rocks: Frontiers in Earth Science, v. 3, doi:10.3389/feart.2015.00004.

Paterson, M.S., and Wong, T.F., 2005, Experimental rock deformation-the brittle field: Springer Science & Business Media.

Peng, S., and Johnson, A.M., 1972, Crack growth and faulting in cylindrical specimens of chelmsford granite: International Journal of Rock Mechanics and Mining Sciences and, v. 9, p. 37–86, doi:10.1016/0148-9062(72)90050-2.

Pollard, D.D., and Segall, P., 1987, Theoretical displacements and stresses near fractures in rock: with applications to faults, joints, veins, dikes, and solution surfacese, *in* In Fracture mechanics of rock, p. 277–347.

Rochette, P., Jackson, M., and Aubourg, C., 1992, Rock magnetism and the interpretation of anisotropy of magnetic susceptibility: Reviews of Geophysics, v. 30, p. 209, doi:10.1029/92RG00733.

Rowe, C.D., and Griffith, W.A., 2015, Do faults preserve a record of seismic slip: A second opinion: Journal of Structural Geology, v. 78, p. 1–26, doi:10.1016/J.JSG.2015.06.006.

Scholz, C.H., 1968, Microfracturing and the inelastic deformation of rock in compression: Journal of Geophysical Research, v. 73, p. 1417–1432, doi:10.1029/JB073i004p01417.

Scholz, C.H., 2002, The Mechanics of Earthquakes and Faulting: New York, Cambridge Univ. Press, 439 p.

Di Toro, G., Nielsen, S., and Pennacchioni, G., 2005, Earthquake rupture dynamics frozen in exhumed ancient faults: Nature, v. 436, p. 1009–1012, doi:10.1038/nature03910.

de Wall, H., Bestmann, M., and Ullemeyer, K., 2000, Anisotropy of diamagnetic susceptibility in Thassos marble: A comparison between measured and modeled data: Journal of Structural Geology, v. 22, p. 1761–1771, doi:10.1016/s0191-8141(00)00105-x.

Weinberger, R., Levi, T., Alsop, G.I., and Marco, S., 2017, Kinematics of Mass Transport Deposits revealed by magnetic fabrics: Geophysical Research Letters, v. 44, p. 7743–7749, doi:10.1002/2017GL074471.

Wilson, J.., Chester, J.., and Chester, F.., 2003, Microfracture analysis of fault growth and wear processes, Punchbowl Fault, San Andreas system, California: Journal of Structural Geology, v. 25, p. 1855–1873, doi:10.1016/S0191-8141(03)00036-1.